Development/Plasticity/Repair

Orchestration of Stepwise Synaptic Growth by K^+ and Ca^{2+} Channels in *Drosophila*

Jihye Lee[1] **and Chun-Fang Wu**[1,2]

[1]Interdisciplinary Program in Neuroscience and [2]Department of Biology, The University of Iowa, Iowa City, Iowa 52242

Synapse formation is tightly associated with neuronal excitability. We found striking synaptic overgrowth caused by *Drosophila* K^+-channel mutations of the *seizure* and *slowpoke* genes, encoding Erg and Ca^{2+}-activated large-conductance (BK) channels, respectively. These mutants display two distinct patterns of "satellite" budding from larval motor terminus synaptic boutons. Double-mutant analysis indicates that BK and Erg K^+ channels interact with separate sets of synaptic proteins to affect distinct growth steps. Post-synaptic L-type Ca^{2+} channels, Dmca1D, and PSD-95-like scaffold protein, Discs large, are required for satellite budding induced by *slowpoke* and *seizure* mutations. Pre-synaptic *cacophony* Ca^{2+} channels and the NCAM-like adhesion molecule, Fasciclin II, take part in a maturation step that is partially arrested by *seizure* mutations. Importantly, *slowpoke* and *seizure* satellites were both suppressed by *rutabaga* mutations that disrupt Ca^{2+}/CaM-dependent adenylyl cyclase, demonstrating a convergence of K^+ channels of different functional categories in regulation of excitability-dependent Ca^{2+} influx for triggering cAMP-mediated growth plasticity.

Introduction

Altered synaptic activity leads to changes in synaptic morphology, providing an effective means to adjust synaptic efficacy. For example, after long-term stimulation simulating the tonic activity patterns, the shape and ultrastructure of pre-synaptic terminals of phasic motoneurons at crayfish neuromuscular junctions (NMJs) are transformed into those resembling tonic terminals (Lnenicka et al., 1986). In addition, prolonged stimulation of lobster motor axons is correlated with pre-synaptic ultrastructural modifications, including increased numbers of active zones (Chiang and Govind, 1986). In parallel, long-term potentiation (LTP) induced by high-frequency nerve stimulation in the mammalian hippocampus can trigger dendritic spine formation in tens of minutes (Engert and Bonhoeffer, 1999).

In line with this activity-dependent synaptic growth, increased excitability from dysfunction of 4-aminopyridine-sensitive, voltage-activated K^+ channels (K_v1 and K_v4) leads to aberrant synaptic growth. In developing *Xenopus* retinal ganglion cells, 4-aminopyridine blockade of K_v channels alters branch outgrowth (McFarlane and Pollock, 2000). Similarly, mutations of K_v1 in *Caenorhabditis elegans* induce abnormal sensory axon branching (Peckol et al., 1999). At *Drosophila* larval NMJs, *Shaker* (*Sh*) mutations affecting K_v1 channels lead to synaptic overgrowth when combined with *ether a go-go* (*eag*) K^+-channel mutations (Budnik et al., 1990) or after modest increase in rearing temperature (Zhong and Wu, 2004). However, beyond 4-aminopyridine-sensitive channels including Sh, little is known about the roles of other K^+ channels in activity-dependent synaptic growth.

Here we report striking synaptic overgrowth indicated by abundant small "satellite" boutons in *slowpoke* (*slo*) (Elkins et al., 1986; Komatsu et al., 1990; Atkinson et al., 1991) and *seizure* (*sei*) (Elkins and Ganetzky, 1990; Titus et al., 1997; Wang et al., 1997) mutants, defective in Ca^{2+}-activated large conductance (BK) and voltage-dependent Erg channels, respectively. Slo (BK) K^+ channels, known to colocalize with Ca^{2+} channels in excitable cells, provide negative feedback onto Ca^{2+}-influx-regulated events, including neurotransmitter release (Salkoff et al., 2006). Sei (Erg) K^+ channels in vertebrates affect cardiac action potential repolarization (Sanguinetti et al., 1995) and regulate neuronal firing frequency adaptation (Sacco et al., 2003).

Importantly, disruption of BK and Erg channels led to abundance of two types of satellites distinct in their morphology, suggesting that they mirror structures differentiated from distinct synaptic growth intermediates trapped by preferential effects of these mutations. These growth steps consisting of initial satellite budding followed by maturation into boutons have been proposed previously based on time-lapse studies of intact larvae (Zito et al., 1999). Recent live imaging of larval NMJs also demonstrated dynamic growth and molecular differentiation of smaller boutons after intense stimulation or high K^+-induced depolarization (Ataman et al., 2008). Our double-mutant analysis further revealed functional associations of BK and Erg channels with distinct pre- and post-synaptic molecules and, more importantly, with Ca^{2+}-influx-induced cAMP signaling in proposed growth and differentiation steps. Together with *Sh*-induced synaptic overgrowth (Zhong et al., 1992; Zhong and Wu, 2004), our data thus indicate that the cAMP signaling pathway acts as a common mediator in excitability-regulated synaptic growth and that dysfunctions of K^+ channels of different prop-

Received July 3, 2010; revised Sept. 3, 2010; accepted Sept. 16, 2010.

This work was supported by National Institutes of Health Grant NS 26528 to C.F.W. We thank Mr. D. Abel and Dr. A. Ueda for technical assistance in TEM experiments. We also thank Drs. N. Atkinson, H. Atwood, H. Bellen, V. Budnik, A. DiAntonio, D. Eberl, B. Ganetzky, R. Ordway, J. Simpson, and J. Wang for providing fly stocks and antibodies and Dr. T. Littleton for providing confocal microscope facility for live imaging.

Correspondence should be addressed to Dr. Jihye Lee, The Picower Institute for Learning and Memory, Massachusetts Institute of Technology, Cambridge, MA 02139. E-mail: jihyelee@mit.edu.

DOI:10.1523/JNEUROSCI.3448-10.2010

 0270-6474/10/3015821-13$15.00/0

erties and distributions can result in modifications of distinct aspects of NMJ growth.

Materials and Methods

Fly stocks. The fly stocks used in this study include the following: wild-type (WT) Canton-S and K^+-channel mutants, *slowpoke* (*slo*^{1}, *slo*^{98}, *slo*^{1}/*slo*^{4}, and *slo*^{98}/*slo*^{4}; *slo*^{4} provided by Dr. N. Atkinson, University of Arizona, Tucson, AZ) and seizure (*sei*^{ts2} and *sei*^{ts2}/*sei*^{ts1}). The following single mutants and their corresponding double-mutant combinations with *slo* and *sei* were examined in this study: *fasciclin II* (*fasII*; *fasII*^{e76} and *fasII*^{e76}/*fasII*^{eB112}; Dr. V. Budnik, University of Massachusetts Medical School, Worcester, MA), *fasII;;slo* (*fasII*^{e76};;*slo*^{1}), *fasII;sei* (*fasII*^{e76}; *sei*^{ts2}), *discs large* (*dlg*; *dlg*$^{X1-2}$/*Y or dlg*$^{X1-2}$/*Df(1)N71*, both of which lack all three PDZ domains; Dr. V. Budnik), *dlg;;slo* (*dlg*$^{X1-2}$/*Y;;slo*^{1}), and *dlg;sei* (*dlg*$^{X1-2}$/*Y;sei*^{ts2}); Ca^{2+}-channel mutants *cacophony* (*cac*; *cac*^{s} and *cac*^{NT27}/*cac*^{s}; Dr. R. Ordway, Pennsylvania State University, University Park, PA), *cac;;slo* (*cac*^{s};;*slo*^{1}, *cac*^{s};;*slo*^{98}, and *cac*^{s};;*slo*^{4}), *cac;sei* (*cac*^{s};*sei*^{ts2}), *Dmca1D* (*Dmca1D*^{AR66}; Dr. D. Eberl, University of Iowa, Iowa City, IA), *Dmca1D;slo* (*Dmca1D*^{AR66};*slo*^{1} and *Dmca1D*^{AR66};*slo*^{98}), and *Dmca1D sei* (*Dmca1D*^{AR66} *sei*^{ts2}; three independent recombinant lines); Na^+-channel mutants *maleless*^{nap} (*nap*^{ts}), *nap;slo* (*nap*^{ts};*slo*^{1} and *nap*^{ts};*slo*^{98}), and *nap sei* (*nap*^{ts} *sei*^{ts2}; three independent recombinant lines); cAMP mutants and transgenic constructs *rutabaga* (*rut*; *rut*^{1}, and *rut*^{1084}), *rut;;slo* (*rut*^{1};;*slo*^{1}), *rut;sei* (*rut*^{1};*sei*^{ts2}), *dunce* (*dnc*; *dnc*^{M14}), *dnc;;slo* (*dnc*^{M14};;*slo*^{1}), *dnc;sei* (*dnc*^{M14};*sei*^{ts2}), *UAS-dunce*$^+$ (*UAS-dnc*$^+$; Dr. H. Atwood, University of Toronto, Toronto, Ontario, Canada), *UAS-dnc*$^+$*/Y; C164-GAL4/+;slo*^{1}, *UAS-dnc*$^+$*/+;mef2-GAL4/+;slo*^{1}*/slo*^{98}, and *UAS-dnc*$^+$*/C155-GAL4;sei*^{ts2}. Pan-neuronal and motoneuron-specific drivers *C155-GAL4* (Bloomington *Drosophila* Stock Center, Indiana University, Bloomington, IN) and *C164-GAL4* (Dr. J. Wang, University of California, La Jolla, CA), respectively, were used for expression of a transgene construct, *UAS-dnc*$^+$, in pre-synaptic neurons. For expression of *UAS-dnc*$^+$ in post-synaptic muscle, *mef2-GAL4* (Bloomington *Drosophila* Stock Center) was used in the *slo* mutant background. *C155-GAL4* was also used to drive pre-synaptic expression of a mutated *sei* transgene (*UAS-sei*^{ts2}; a generous gift from Drs. J. Simpson, Janelia Farm Research Campus, Ashburn, VA and B. Ganetzky at University of Wisconsin–Madison, Madison, WI). UAS-RNAi transgenes specifically targeting *slo* and *sei* (*UAS-slo*-RNAi, #6723 and #104421; *UAS-sei*-RNAi, #104698 and #3606; Vienna *Drosophila* RNAi Center) were used in combinations with multiple neuronal and muscular GAL4 drivers (*C155* and *C164* for neuronal drivers; *Mhc*, *C179*, and *mef2* for muscular drivers) to reproduce mutant phenotypes in the WT background. Whenever possible, we used multiple alleles or independent isolates of each gene in phenotypic characterization to minimize the contributions from genetic variants of unidentified loci. Our results indicate overall similarities between multiple alleles in the numbers of mature boutons and satellites (supplemental Table S1, available at www.jneurosci.org as supplemental material).

All stocks were raised on conventional fly medium and maintained at room temperature (RT). In experiments for long-term high-temperature (HT) rearing, adult flies were kept at RT in fresh food vials for egg laying for 1 d, which were subsequently placed in a 29°C incubator for additional 4 to 5 d to cover entire larval development. For a short-term HT treatment, vials were kept at RT for 5–7 d until the majority of the larval population reached the third-instar stage and were then placed in a 29°C incubator for 5 h before dissection.

Immunohistochemistry. Larvae were prepared as described previously (Lee et al., 2008). The primary antibodies used include monoclonal Fasciclin II [FasII; 1D4; 1:4; Developmental Studies Hybridoma Bank (DSHB)], Bruchpilot (Brp; NC82; 1:250; DSHB), and α-tubulin antibodies (clone 1A; 1:400; Sigma-Aldrich), and polyclonal Discs large (Dlg; 1:20,000; Dr. V. Budnik), glutamate receptor subunit IIC (DGIuRIIC; 1:1000; Dr. A. DiAntonio, Washington University, St. Louis, MO), Nervous wreck (Nwk; 1:2000; Dr. B. Ganetzky), and dynamin-associated protein, 160 kDa (Dap160; 1:200; Dr. H. Bellen, Baylor College of Medicine, Houston, TX). The pre-synaptic terminals were visualized by FITC- or Texas Red-conjugated horseradish peroxidase (HRP) antibody (1:50; Jackson ImmunoResearch).

Imaging and analysis. Images of NMJs on muscle 4 from abdominal segments 3 through 7 were collected using an M1024 confocal microscope (Bio-Rad). The collapsed *Z*-stacked images of type Ib NMJs recognized by anti-HRP signals were compiled by ImageJ software (NIH Image) and analyzed for the numbers of primary mature boutons, satellites, and terminal branches. A satellite was defined as a bouton of smaller size than adjacent mature boutons deviating from the main trajectory of terminal branches. Two types of satellites were classified based on the following criteria: "type B" satellites resemble yeast budding without a clear constriction, whereas "type M" satellites display a neck-like constriction separating mature boutons and satellites. A branch was defined as a projection that contains two or more boutons in series separated by clear interbouton regions. A branch segment was indicated as a region between two adjacent branching points, and ascending orders were given to the next level of branch segments at each branching point. The arbitrary branch index reflecting the complexity of branching patterns was calculated based on the following formula: branch index = 1 × (the number of first-order branch segments) + 2 × (the number of second-order branch segments) + 3 × (the number of third-order branch segments) + 4 × (the number of branch segments of an order higher than the third).

For comparison of distributions of FasII and Dlg between type B and M satellites, each NMJ was manually traced for FasII and Dlg immunoreactivity with the pixel intensities measured from each satellite and four to five adjacent mature boutons within the same NMJ. The relative intensity ratios (percentage intensity from satellites/mature boutons) were then compared between the entire populations of type B and M satellites for *slo* and *sei* mutants.

Electron microscopy. Larvae dissected in hemolymph-like (HL) 3.1 saline were superfused for 15 min with fixative (0.1 M sodium cacodylate buffer, 2.5% glutaraldehyde, and 2.5% formaldehyde, pH 7.2) and then stored in a vial for 2 h at RT. After fixation, the tissue was rinsed in the buffer solution followed by postfixation in buffered 1% osmium tetroxide for 1 h and a 15 min rinse in buffer. Subsequent dehydration was performed in 30–100% ethanol series followed by clearing in propylene oxide and embedding in plastic (Polybed 812; Polysciences). The plastic block cured in a 60°C oven for 1–2 d was sectioned, placed on copper grids, and double stained with uranyl acetate and lead citrate. NMJ electron micrographs were taken at a magnification of 10,000 to 20,000.

Statistical analysis. For comparison between two genotypes, two-tailed *t* test was routinely performed against the null hypothesis of equal values between two genotypes, unless indicated otherwise. A p value <0.05 was considered significantly different. All statistical analyses were performed using Origin software (version 6.0; OriginLab).

Results

Aberrant synaptic growth patterns in *slowpoke* and *seizure* K^+-channel mutants

The stereotypic innervation patterns of *Drosophila* larval NMJs, with identifiable motoneurons and muscle fibers, facilitate detection of morphological modifications and have enabled quantitative studies of the regulatory mechanisms underlying activity- and excitability-dependent synaptic growth (Budnik et al., 1990; Sigrist et al., 2003). In this study, we investigated striking NMJ phenotypes in *slo* and *sei* mutants (Fig. 1), which displayed abundant small boutons, termed "satellites," budding from the larger primary boutons along the branch axis (Fig. 1*B*, arrows and arrowheads). Such aberrant outgrowth was found at both type Ib and Is NMJs (Johansen et al., 1989; Atwood et al., 1993) in different muscles, e.g., 6/7 (Fig. 1*A*) and 4 (Fig. 1*B*, type Ib only). To facilitate quantitative analysis, we focused on type Ib NMJs in muscle 4, which displayed a stereotypic branching pattern with fewer boutons of larger sizes. During closer examination, two distinct types of satellites were observed, one without a clear constriction between satellites and primary boutons, resembling yeast budding (Fig. 1*B*, arrowheads) (hereafter, "type B satellite") and the other with a short but clear constriction or "neck" (Fig. 1*B*, arrows) (hereafter, "type M satellite"). Our results indicated more abundant type B satellites in *slo* mutants in contrast to a

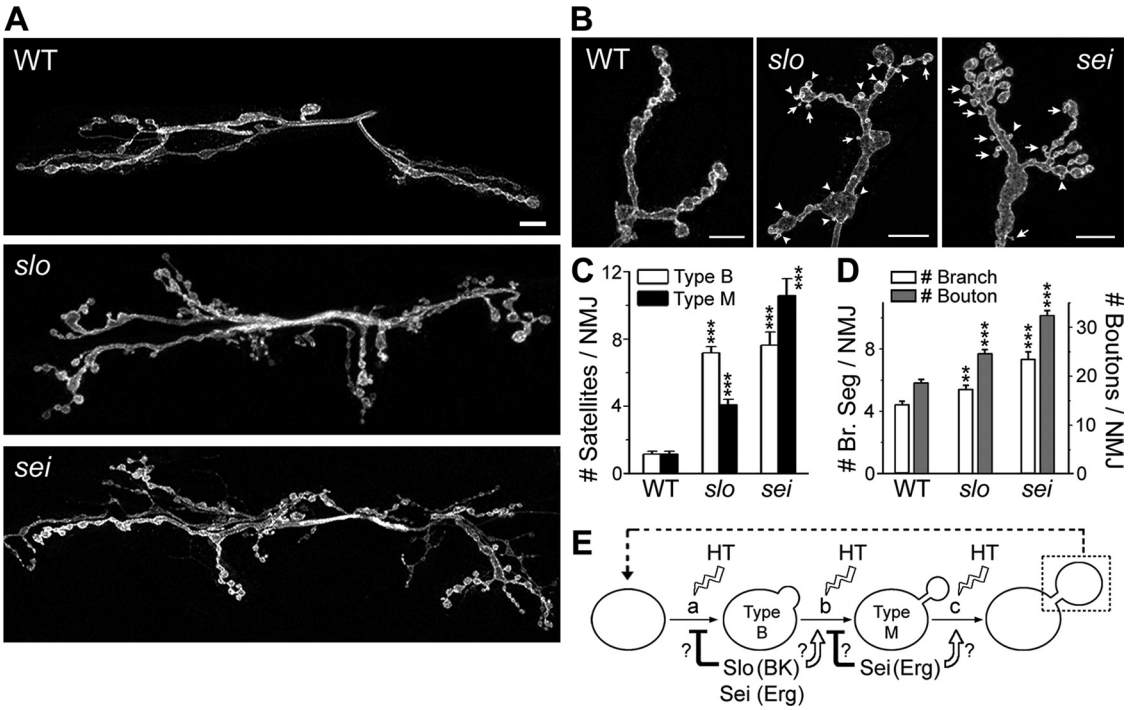

Figure 1. Aberrant synaptic growth induced by *slo* and *sei* K^+-channel mutations. ***A***, ***B***, Representative anti-HRP immunostaining of WT, *slo*, and *sei* larval NMJs in muscles 6 and 7 (***A***) and muscle 4 (M4; type Ib only; ***B***) of abdominal segments 3 or 4. Note the more extensive branching at *slo* and *sei* NMJs (***A***) and small "satellite" boutons in these mutants budding from larger, primary synaptic boutons either with (type M, arrows) or without (type B, arrowheads) a clear constriction (***B***). Fluorescent micrographs in this and subsequent figures are collapsed confocal *Z*-stacks. Scale bars: ***A***, 10 μm; ***B***, 5 μm. ***C***, ***D***, Pooled data are shown for the numbers of types B and M satellites (***C***) and of mature primary boutons and terminal branches [branch segments (Br. Seg)] (***D***) per type Ib M4 NMJ. The number of NMJs (larvae) examined is as follows: 91 (30) for WT, 107 (34) for *slo*, and 38 (11) for *sei*. $^{**}p < 0.01$; $^{***}p < 0.001$ (one-way ANOVA). ***E***, Model of sequential synaptic growth process, from initial budding (type B satellites; step a) to maturation into type M satellites (step b) and formation of primary boutons (step c). Open arrows and closed bars indicate the alternative possibilities of promoting or restraining actions, respectively, exerted by these K^+ channels at individual steps that might explain the mutant phenotypes (see Results). Facilitated growth by HT treatment and reiteration of a growth cycle (dashed line) are indicated. Error bars indicate mean ± SEM.

majority of type M satellites in *sei* mutants (Fig. 1*C*). These alterations were accompanied by increases in the synaptic bouton number and terminal branching for both mutants (Fig. 1*D*). Both *sei* and *slo* mutants were first identified as temperature-sensitive mutants because of more evident behavioral manifestations at HT (Elkins et al., 1986; Elkins and Ganetzky, 1990). However, our experiments performed at RT revealed abundant satellites in both mutants, demonstrating the severe effects of dysfunctions of the Erg and BK channels, separately encoded by the two genes.

The satellites abundant in *slo* and *sei* mutants are morphologically similar to primordial boutons detected during normal development, which mature into primary boutons and form new branches (Zito et al., 1999). Such similarity raised the possibility that satellites may represent arrested structural intermediates accumulated during synaptic growth that are rarely seen in mature third-instar WT larvae (Fig. 1*C*). We proposed a working hypothesis in an attempt to link these putative structural intermediates in a sequential growth process. Similar to the scheme proposed for normal bouton development (Zito et al., 1999), we assumed that type B satellites are derived from initial budding, whereas type M satellites reflect derivatives from intermediates of a more mature state that further differentiate and transform into full-grown boutons (Fig. 1*E*).

Given that type B satellites recapitulate the initial budding process, two possibilities may be invoked to explain their abundance in *slo* mutants. First, Slo channel activity may promote the formation of type M satellites (Fig. 1*E*, open arrow, step b). A retarded transformation in *slo* mutants should lead to accumulation of type B satellites, but with a fewer number of type M satellites and mature boutons. This scenario contradicts our observations of a significant fraction of type M satellites together with more mature boutons and terminal branches in *slo* (Fig. 1*C*,*D*). Conversely, Slo channels may normally serve as a restraining factor, preventing excessive budding from mature boutons (Fig. 1*E*, closed bar, step a). Thus, *slo* mutations may unleash the growth, leading to accumulation of large proportions of type B satellites. This would also enhance conversion of type B satellites into type M satellites or even mature boutons at a limited rate, which appears to be consistent with the observed *slo* phenotypes (Fig. 1*C*,*D*).

In contrast, *sei* mutants were characterized by more abundant type M than B satellites, along with significantly enhanced bouton and branch formation (Fig. 1*C*,*D* for sei^{ts2}) (to a lesser extent in sei^{ts2}/sei^{ts1} mutants; data not shown). Abundant type B satellites in *sei* mutants comparable to *slo* suggest a similarly unleashed growth in the earlier step (Fig. 1*E*, step a), indicating a restraining action of Sei as well as Slo K^+ channels. However, the excessive accumulation of type M satellites implicates an additional action of Sei channels in later steps. First, a restraining action on transformation of type B into M satellites may be considered (Fig. 1*E*, closed bar, step b). In this case, mutations in Sei channels would result in more type M satellites and mature boutons with depletion of type B satellites to some extent. However, this prediction contradicts the observed *sei* phenotype with abundant type B satellites comparable to *slo* (Fig. 1*C*). Our result thus favors an alternative possibility of Sei channels in facilitating maturation of type M satellites into mature boutons and terminal

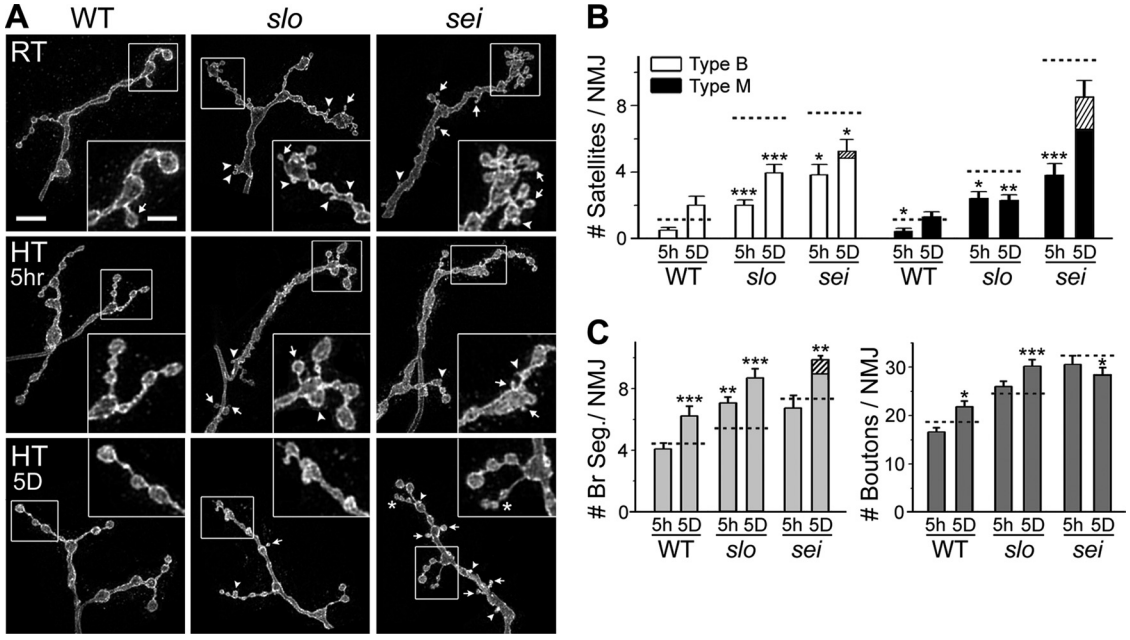

Figure 2. Dynamic synaptic growth regulation in *slo* and *sei* mutants revealed by short- and long-term exposure to high rearing temperature. ***A***, Representative type Ib NMJs in muscle 4 (M4) of WT, *slo*, and *sei* larvae reared at RT (top) and after short-term (5 h; middle) or long-term [5 d (5D); bottom] exposure to high temperature (29°C). Examples of types B (arrowheads) and M (arrows) satellites are indicated. Note branches consisting predominantly of type M satellites (asterisks) that are found only in long-term, HT-treated *sei* larvae. Scale bars: ***A***, 10 μm; insets, 5 μm. ***B***, ***C***, Pooled data for the numbers of types B and M satellites (***B***), terminal branches, and mature primary boutons (***C***) at type Ib M4 NMJs are shown for short- and long-term HT-treated WT, *slo*, and *sei* larvae. The control values at RT (from Fig. 1 for each genotype) are indicated by dashed lines. The portions of HT-induced small type B or M satellites forming strings at *sei* NMJs are indicated as hatched bars. The numbers of NMJs (larvae) examined are as follows: after HT for 5 h, WT, 23 (7); *slo*, 26 (7); *sei*, 12 (3); after HT for 5 d, WT, 22 (6); *slo*, 35 (8); *sei*, 24 (6). $*p < 0.05$; $**p < 0.01$; $***p < 0.001$ [*t* test for RT vs HT (5 h or 5 d) within each genotype]. Error bars indicate mean ± SEM.

branches (Fig. 1*E*, open arrow, step c). Thus, mutations of Sei channels may partially stunt the development and lead to excessive accumulation of type M satellites, along with enhanced, although less extreme, overgrowth of type B satellites, consistent with the observed *sei* phenotypes (Fig. 1). Notably, *sei* mutants displayed significantly enhanced branching patterns along with robust increase in mature bouton numbers (Fig. 1*D*), indicating that *sei* mutations do not fully prevent type M satellites from entering the successive growth steps. These hypotheses were further examined with additional manipulations, such as HT treatments and double-mutant combinations (see below).

We then examined *sei;slo* double mutants to further explore the differential effects of *sei* and *slo* in the proposed stepwise growth processes. When compared with single mutants, the combined mutational effects of the two genes in *sei;slo* were not simply additive, with a further enhancement of some *slo*, but not *sei*, phenotypes. Apparently, satellite abundance was less extreme in *sei;slo* double mutants compared to *sei* mutants. There was a slight, but not significant, reduction in the numbers of both types B and M satellites [$p > 0.10$, mean ± SEM (*n*), *sei;slo* vs *sei*, 5.25 ± 0.86 (20) vs 7.63 ± 0.80 (38) for type B; 7.42 ± 1.33 (20) vs 10.58 ± 1.02 (38) for type M]. In contrast, the numbers of type M (but not type B) satellites and mature boutons were significantly greater in *sei;slo* compared to *slo* [mean ± SEM (*n*), *sei;slo* vs *slo*, 7.42 ± 1.33 (20) vs 4.09 ± 0.32 (107), $p < 0.01$, for type M; 5.25 ± 0.86 (20) vs 7.18 ± 0.37 (107), $p > 0.10$, for type B satellites; 28.70 ± 1.84 vs 24.67 ± 0.80, $p < 0.05$, for mature boutons]. The enhanced overgrowth of these two structures in double mutants beyond the levels in *slo* is consistent with the idea that Sei K^+ channels exert influences on the later steps of the synaptic bouton growth processes (Fig. 1*E*). The lack of further overgrowth in *sei;slo* beyond the levels in *sei* suggests the existence of a saturable capacity, or an optimal activity level for promotion of the excitability-associated synaptic growth examined here. Possible explanations include potential overlapping actions of Sei and Slo K^+ channels onto activity-dependent, common downstream effectors such as Ca^{2+} and cAMP (see below).

Dynamic growth process revealed by high rearing temperature in *slo* and *sei* mutants

HT treatment on *slo* and *sei* mutants revealed the time scales in the dynamic growth process described above. Although 2 h exposures to HT (29°C) failed to induce significant morphological changes (data not shown), both types of satellites in these mutants were apparently suppressed by longer incubation (5 h) (see Materials and Methods) (Fig. 2*A*). Whereas the frequency of type B, rather than type M, satellites was drastically reduced in *slo* mutants, type M satellites were reduced to a greater extent in *sei* mutants (Fig. 2*B*), in line with the relative abundance of each type of satellites in these two mutants (Fig. 1*C*) and the proposed major actions of Slo and Sei channels at RT (Fig. 1*E*). Importantly, HT treatment for 5 h further increased the number of branches in *slo* mutants (Fig. 2*C*). Unlike *slo* and *sei* mutants, WT failed to respond to the same 5 h HT treatment (Fig. 2), consistent with a previous report (Sigrist et al., 2003). These results thus indicate that these mutations provided a sensitized condition to expose the temperature dependency of individual growth steps (Fig. 1*E*).

In parallel, chronic HT treatment (5 d, sufficient to cover the entire larval development) induced significant increases in both bouton and branch numbers in WT, consistent with previous reports (Sigrist et al., 2003; Zhong and Wu, 2004), despite no significant changes in the rare occurrence of satellites (Fig. 2). Unlike WT, chronic HT-treated *slo* mutants displayed signifi-

cantly reduced frequency of both types of satellites (Fig. 2*B*) along with increased mature bouton and branch numbers (Fig. 2*C*). These results thus corroborate the above short-term HT effects, suggesting facilitated transformation of *slo*-induced satellites into primary boutons and terminal branches after raising the temperature.

In chronic HT-treated *sei* mutants, we observed a unusual population of terminal branches consisting of thin strings of type M (and occasionally type B) satellites that were absent in HT-treated WT or *slo* larvae (Fig. 2*A*, asterisks, *B*, hatched bars), contributing to enhanced branching complexity (Fig. 2*C*, hatched bar). This observation is in line with a specific role of Sei channels in later growth steps (compare Fig. 1*E*, step c), but we also detected a contrasting decrease in primary bouton number in chronic HT-treated *sei* larvae (Fig. 2*C*). How the further enhanced branching took place in the expense of bouton formation remains unclear, awaiting further investigation.

Together, these acute and chronic HT-induced modifications indicate that elevated temperature may promote synaptic restructuring or growth, providing a force to overcome barriers at specific steps caused by dysfunction of Sei and Slo K^+ channels.

Dominant mutational effects of *sei* and *slo* on synaptic growth

Sei Erg and Slo BK channels, like many other K^+ channels, are thought to be composed of four identical subunits (Hille, 2001). Thus, a mixture of mutant and wild-type subunits in a multimeric assembly in heterozygous mutants could lead to a dominant-negative effect, altering the function of heteromeric channels that contain one or more mutant subunit and sparing only a minority of channels that consist strictly of WT subunits. For example, such dominant effect on HT-induced seizure and paralytic behavior was evident in heterozygous sei^{ts2}/+ flies carrying a point mutation in the pore domain of the channel (Titus et al., 1997; Wang et al., 1997), comparable to those observed in the homozygote (sei^{ts2}/sei^{ts2}) (Jackson et al., 1985). Therefore, we have examined the morphological phenotypes of sei^{ts2}/+ and *slo*/+ in comparison with sei^{ts2}/sei^{ts2} and *slo/slo*, respectively, at larval NMJs.

Importantly, we observed dominant effects on satellite and bouton formation in sei^{ts2}/+ as well as *slo*/+ heterozygotes (supplemental Table S2, available at www.jneurosci.org as supplemental material). Larvae heterozygous for two alleles of *slo* (slo^1/+ and slo^{98}/+) showed increases in all of the parameters we examined, including the numbers of both types of satellites, mature boutons, and branch segments, to levels comparable to the homozygous counterpart (*slo/slo*). However, larvae heterozygous for a null allele, slo^4/+ (Atkinson et al., 1991), did not display significant enhancement in these growth parameters except for bouton formation (supplemental Table S2, available at www.jneurosci.org as supplemental material). Such contrasting phenotypes between null (slo^4/+) and non-null alleles (slo^1/+ and slo^{98}/+) of *slo* in the heterozygote are consistent with the idea that dominant-negative effects can result from the incorporation of mutated subunits in the combinatorial assembly of a multimeric channel and indicate a high sensitivity of these growth processes to dysfunction of Slo K^+ channels. Considering a tetrameric subunit assembly of Slo channels, the fraction of intact channels strictly composed of WT subunits in slo^1/+ or slo^{98}/+ larvae could be significantly lower than that expected (50%) in slo^4/+, consistent with their relative phenotypic severity (supplemental Table S2, available at www.jneurosci.org as supplemental material). Similar interference by mutated *Sh* subunits beyond the simple gene-dosage effects of null mutations has been documented previously in voltage-clamp measurements for Sh K^+ current amplitude in *Drosophila* larval muscle fibers (Haugland and Wu, 1990).

In the case of sei^{ts2}/+ larvae, we observed a significant increase in the number of mature boutons and type B satellites, but the number of type M satellites and branch segments remained comparable to WT (supplemental Table S2, available at www.jneurosci.org as supplemental material). These results indicate differential degrees of dominant mutational effects on each growth step, i.e., the initial budding step with a higher sensitivity to Sei channel dysfunction versus the later growth steps such as branch formation more resistant to the same degrees of dysfunction in these heterozygous larvae.

Synaptic ultrastructure and protein distribution in *slo* and *sei* satellites

We then examined the potential structural distinctions between two types of satellites, indicative of regulatory mechanisms differentially affected by *slo* and *sei* mutations. Both types of satellites contained synaptic vesicles, electron-dense synaptic area and T-bars, and subsynaptic reticulum, a specialized folding of post-synaptic muscle membranes (Jan and Jan, 1976) (Fig. 3*A*), similar to normal growing boutons (Zito et al., 1999) and mature synapses (Atwood et al., 1993). The presence of active zones in these satellites was also detected when an antibody (NC82) against Bruchpilot, a protein important for integrity of T-bars (Wagh et al., 2006), was used for visualizing active zones at a light-microscopic level (Fig. 3*C*). In addition to the similarity in ultrastructure, immunostaining demonstrated post-synaptic association of glutamate receptor clusters containing DGluRIIC subunits with both types of satellites (supplemental Fig. S1, top, available at www.jneurosci.org as supplemental material).

Aside from these similarities, distinct microtubule distributions between the two types of satellites were indicated by α-tubulin immunostaining (Fig. 3*B*), in contrast to comparable phalloidin-labeled actin networks (data not shown). Although there was no detectable microtubule structure in type B satellites (Fig. 3*B*, arrowheads), some type M satellites displayed a loop-like microtubule arrangement (Fig. 3*B*, arrows) that is known to be associated with structurally stable, mature synaptic boutons (Roos and Kelly, 1998). When the data from multiple satellites were compared for the presence of filamentous or loop-like tubulin structures, we were unable to detect any type B satellites with these structures in both *slo* (0 of 60) and *sei* (0 of 28) mutants. In contrast, such features were evident in subsets of type M satellites in both mutants, with a higher fraction in *sei* than *slo* (15 of 59 for *sei* vs 4 of 54 for *slo*). This is consistent with our model that type M satellites, abundant in *sei* mutants, mirror more advanced structural intermediates than type B satellites (Fig. 1*E*).

In previous studies, satellites are also frequently observed in mutants defective in Nwk and Dap160, which affect actin dynamics and membrane recycling (Coyle et al., 2004; Koh et al., 2004; Marie et al., 2004), as well as in other endocytic mutants (Dickman et al., 2006). We thus investigated potential alterations in their distributions in *slo* and *sei* mutants. However, immunoreactivities against Nwk and Dap160 were clearly detected in both types of satellites in mutants, similar to those in adjacent primary boutons (supplemental Fig. S1, available at www.jneurosci.org as supplemental material), suggesting that satellite formation induced by these K^+-channel mutations is not likely attributable to alterations in actin cytoskeleton and membrane recycling caused by gross differences in the levels of Nwk and Dap160. Whether *slo*

and *sei* mutations alter fine-tuning of these cellular processes during development awaits further investigation.

It is interesting to note that a previous live-imaging study has documented the sighting of rapid growth of synaptic terminals at larval NMJ within minutes after either high-frequency electrical stimulation or high K^+-induced depolarization (Ataman et al., 2008). However, these newly formed boutons of a smaller size, referred to as "ghost boutons," were not equipped with pre- and post-synaptic markers, indicating a lack of synaptic differentiation. Accumulation of putative pre-synaptic active zones markers and post-synaptic glutamate receptor clusters was evident only after hours to days, indicating slower differentiation in the maturation and stabilization processes. Significantly, such a slow differentiation time course is consistent with HT-induced modulation we observed over the span of hours and days (Fig. 2).

Additional exploration revealed abundant satellites well differentiated with pre- and post-synaptic markers, including Dlg and FasII in addition to DGluRIIC, contrasting with "ghost boutons" in their youth (see below). Thus, *slo* and *sei* satellites may reflect the trapped transient growth steps undergoing subsequent molecular and ultrastructural differentiation. The abundance of these satellites may be derived from stabilization and preservation of growth intermediates described in time-lapse imaging of developing NMJs in intact larvae (Zito et al., 1999).

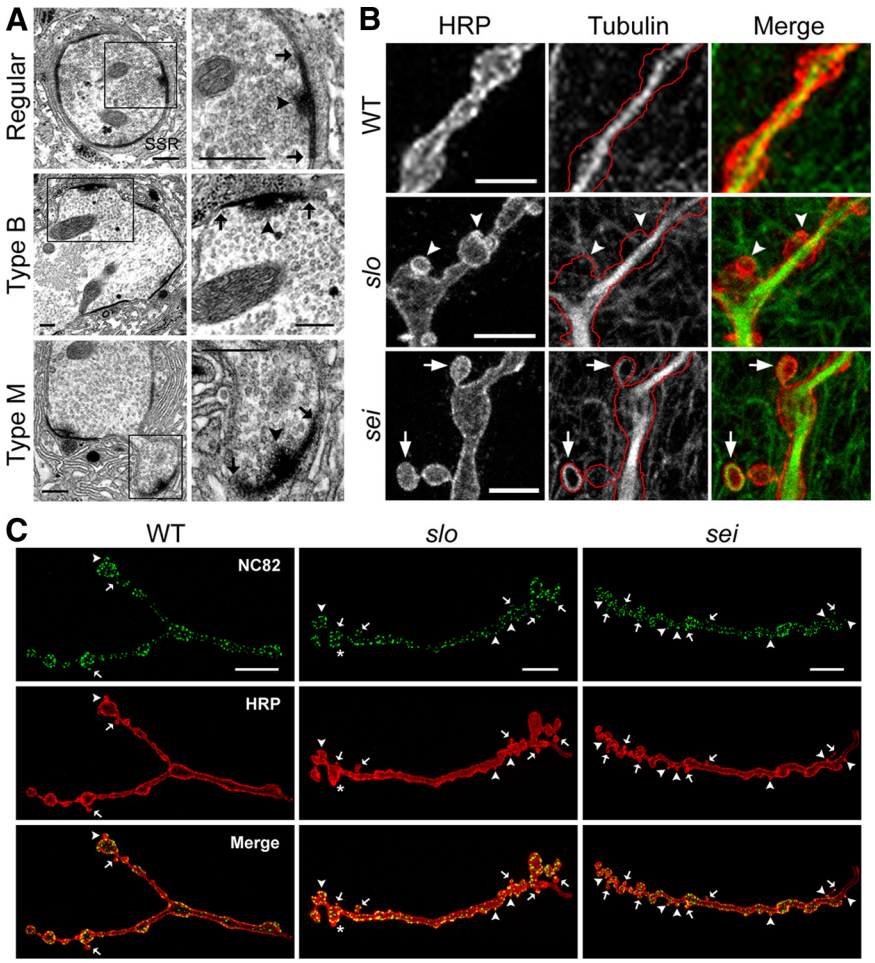

Figure 3. Synaptic ultrastructure and microtubule networks in *slo* and *sei* satellites. ***A***, Electron microscopy images of mature boutons and satellites found in *slo* and *sei* mutants. In contrast to smooth contour of a WT bouton (top), the contours of *slo* and *sei* boutons appear irregular because of the presence of types B (middle) and M (bottom) satellites. Note the presence of electron-dense membrane areas (demarcated by arrows) and T-bar specializations (arrowheads) associated with synaptic active zones, as well as synaptic vesicles, in both types of satellites. The boxed region in the left column is magnified on the right. ***B***, Confocal images of type Ib NMJs in muscle 4 (M4) of WT, *slo*, and *sei* larvae displaying networks of microtubules revealed by α-tubulin immunoreactivity (middle). Pre-synaptic bouton contours (red lines) are traced from anti-HRP images (left) against α-tubulin images (middle). Note the lack of clear tubulin immunoreactivity within type B satellites (*slo*; arrowheads), in contrast to a distinct loop structure in type M satellites (*sei*; arrows). ***C***, Confocal images of type Ib NMJs in M4 of WT, *slo*, and *sei* larvae displaying overall distributions of active zones visualized by NC82 antibody against Brp, a protein important for T-bar integrity at active zones (top). General morphology of each NMJ is revealed by double staining of HRP at the same NMJs (middle). Note clear NC82 signals in type B (arrowheads) and M (arrows) satellites with a rare exception (asterisk). Scale bars: ***A***, 0.5 μm; ***B***, 5 μm; ***C***, 10 μm.

Differential contributions of FasII and Dlg to satellite formation in *slo* and *sei* mutants

In addition to microtubule networks described above, two types of satellites were further distinguished by immunostaining of a scaffold protein, Dlg (Lahey et al., 1994) and cell-adhesion molecule FasII (Bastiani et al., 1987), two synaptic proteins interacting during synaptic growth in *Drosophila* embryos (Kohsaka et al., 2007). Within the same NMJ preparation, heavy decoration of Dlg immunoreactivity was observed in type B satellites as well as adjacent mature boutons (Fig. 4*A*, arrowheads), whereas it was significantly reduced around type M satellites in both *slo* and *sei* mutants (Fig. 4*A*, arrows; supplemental Fig. S2, available at www.jneurosci.org as supplemental material) ($p < 0.001$ between type B and M satellites). In contrast, the level of FasII immunofluorescence was significantly higher for both types of satellites compared to that in mature boutons (supplemental Fig. S2, available at www.jneurosci.org as supplemental material), which may be attributable in part to a larger surface-to-volume ratio of satellites. FasII levels were comparable between two types of satellites despite a small, but statistically significant, difference in immunoreactivity of type M satellites at *sei* NMJs (supplemental Fig. S2, available at www.jneurosci.org as supplemental material).

These results demonstrate differential distribution of Dlg, but not FasII, between type B and M satellites, and thus suggest potential differences in Dlg- and FasII-dependent regulation in the sequential steps of synaptic growth. We examined double-mutant combinations and found striking differential effects of *fasII* mutations on *slo* and *sei* satellites. Significantly, satellite frequency in *fasII;;slo* remained comparable to *slo*, whereas satellites in *fasII;sei* were significantly reduced from the *sei* level, more pronouncedly for type M than type B satellites (Fig. 4*C*). This is in contrast to the observation of similar distribution profiles of FasII immunoreactivity in both *slo* and *sei* single mutants. Such differential suppression of *sei* phenotypes by *fasII* was also reflected in the frequency of mature boutons (supplemental Table S1, available at www.jneurosci.org as supplemental material) and complexity of terminal branches (Fig. 4*B*, branch index) (see Materials and Methods) when *fasII;;slo* and *fasII;sei* were compared. The bouton number was slightly reduced in *fasII;;slo* dou-

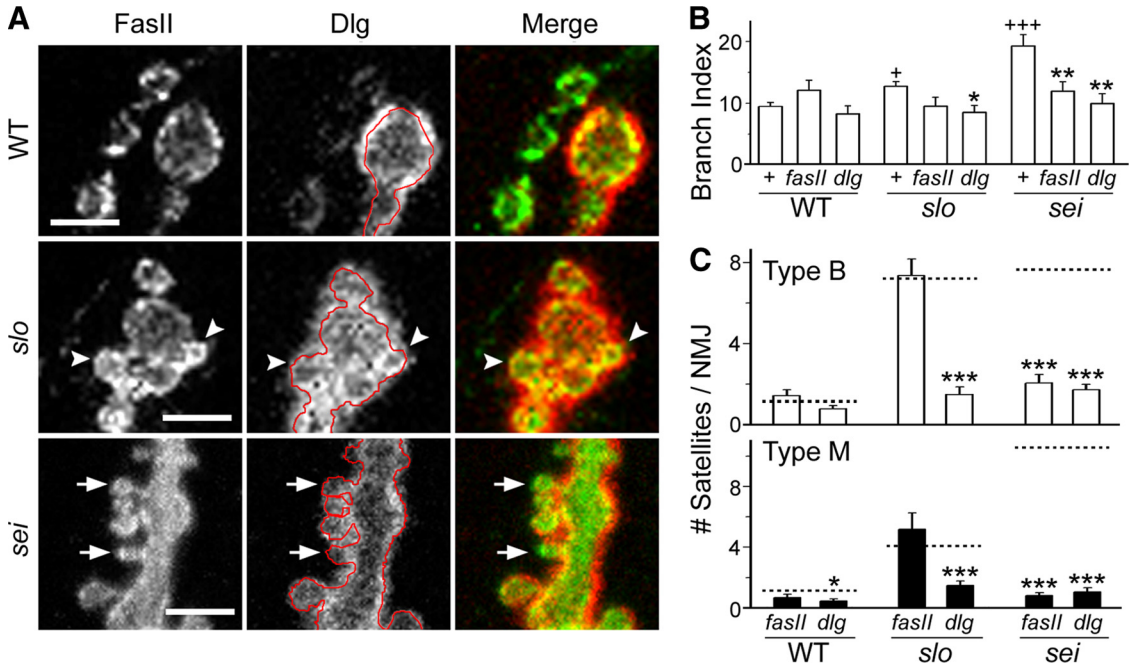

Figure 4. Distribution of Dlg scaffold and FasII adhesion proteins and suppression of *slo* and *sei* satellites by *dlg* and *fasII* mutations. ***A***, Immunoreactivity against FasII (left) and Dlg (middle) at WT (types Ib and Is), *slo*, and *sei* (type Ib only) muscle 4 NMJs. The contour of boutons outlined by FasII immunoreactivity in red (middle) indicates sparse post-synaptic Dlg immunoreactivity around type M satellites (*sei*; arrows) in contrast to profuse staining surrounding type B satellites (*slo*; arrowheads) and mature boutons. Scale bars: 5 μm. ***B***, ***C***, Quantification of branching complexity (***B***; branch index) (see Materials and Methods) and frequency of type B and M satellites (***C***, open and closed bars, respectively) for WT, *slo*, *sei*, and their double-mutant combinations with *fasII* or *dlg*. Dashed lines in ***C*** indicate satellite frequencies for WT, *slo*, and *sei* larvae (compare Fig. 1*C*). Note drastically reduced satellite frequency in *dlg;;slo* and *dlg;sei* mutants in contrast to a selective reduction only in *fasII;sei* but not *fasII;;slo*. The numbers of NMJs (larvae) examined are as follows: 91 (30) for WT; 19 (5) for *fasII*; 22 (7) for *dlg*; 107 (34) for *slo*; 22 (6) for *fasII;;slo*; 23 (7) for *dlg;;slo*; 38 (11) for *sei*; 22 (5) for *fasII;sei*; 18 (6) for *dlg;sei*. $^{+}p < 0.05$; $^{+++}p < 0.001$ (*t* test for WT vs *slo* or *sei*). $*p < 0.05$; $**p < 0.01$; $***p < 0.001$ (*t* test for WT, *slo*, or *sei* vs double mutants within each group). Error bars indicate mean ± SEM.

ble mutants, but a similar reduction was seen in *fasII* (compared to WT, $p < 0.05$) (cf. Schuster et al., 1996). However, far more reduction was observed in *fasII;sei* (supplemental Table S1, available at www.jneurosci.org as supplemental material). This preferential modification of *sei* rather than *slo* phenotypes by *fasII*, i.e., significant suppression of type M satellite formation and its maturation, suggests a tight interaction between FasII and Sei channels at the later steps in the growth process (Fig. 1*E*, step c). Additionally, significantly reduction of type B satellites in *fasII;sei* double mutants indicates that interaction of FasII and Erg channels occur in an earlier growth step as well (Fig. 1*E*, step a).

In contrast to *fasII*, a *dlg* mutation reduced not only type B, but also type M satellites in both *dlg;;slo* and *dlg;sei* mutants close to the WT level (Fig. 4*C*). Furthermore, such reduced satellite frequency in double mutants was correlated with fewer mature boutons (supplemental Table S1, available at www.jneurosci.org as supplemental material) ($p < 0.001$ for *slo* vs *dlg;;slo* and *sei* vs *dlg;sei*) and with simpler branching patterns indicated by the reduced branching index when compared to *slo* and *sei* single mutants (Fig. 4*B*). These results thus imply that Dlg may be involved in the initial step of satellite formation induced by both *sei* and *slo* mutations (Fig. 1*E*, step a). Interfering with initial formation of type B satellites, the *dlg* mutation could prevent their transformation into type M satellites and mature boutons, consistent with our results (Fig. 4; supplemental Table S1, available at www.jneurosci.org as supplemental material).

Along with significant suppression of satellites by *dlg* mutations (Fig. 4*C*), heavier decoration of Dlg in type B than in type M satellites in both *slo* and *sei* NMJs (Fig. 4*A*; supplemental Fig. S2, available at www.jneurosci.org as supplemental material) also raised a possibility that a manipulation of the Dlg level may differentially modify type B and M satellites. This idea was tested in *slo* mutants, which display higher frequencies of type B than type M satellites (Fig. 1*C*), by overexpressing WT *dlg* transgene tagged with EGFP (*UAS-dlg$^+$-EGFP*). Since the majority of immunoreactivity against endogenous Dlg is detected from the post-synaptic muscles surrounding nerve terminals at NMJs, we expressed this transgene using a muscle-specific GAL4 driver, *mef2* (Gossett et al., 1989; Lilly et al., 1994). Indeed, the expression profiles of *UAS-dlg$^+$* recognized by EGFP closely resembled those observed for endogenous Dlg in WT larvae (data now shown). Notably, in contrast to the severe suppression of both type B and M satellites in *dlg;;slo* (Fig. 4*C*), overexpression of *dlg$^+$* induced a more pronounced reduction in type B satellites (supplemental Fig. S3, available at www.jneurosci.org as supplemental material) (*slo* vs *UAS-dlg$^+$(in muscle);slo*; $p < 0.001$ for type B vs $p > 0.05$ for type M). As a result, the numbers of remaining type B and M satellites became similar, and there were fewer satellites in total (supplemental Fig. S3, available at www.jneurosci.org as supplemental material). More importantly, in contrast to a reduction observed in *dlg;;slo* compared to *slo*, the number of mature boutons was significantly enhanced in *slo* larvae expressing post-synaptic *dlg$^+$* (supplemental Fig. S3, available at www.jneurosci.org as supplemental material). Selective decrease in type B satellite frequency coupled with enhanced bouton formation raises a possibility that excessive Dlg expressed in the post-synaptic muscle may provide a platform to promote conversion of type B satellites to type M, which can mature into boutons. This represents an interesting parallel to the modulation induced by HT treatment in *slo* mutants (compare Fig. 2*B*,C, with supplemental Fig. S3, available at www.jneurosci.org as supplemental material), demonstrating

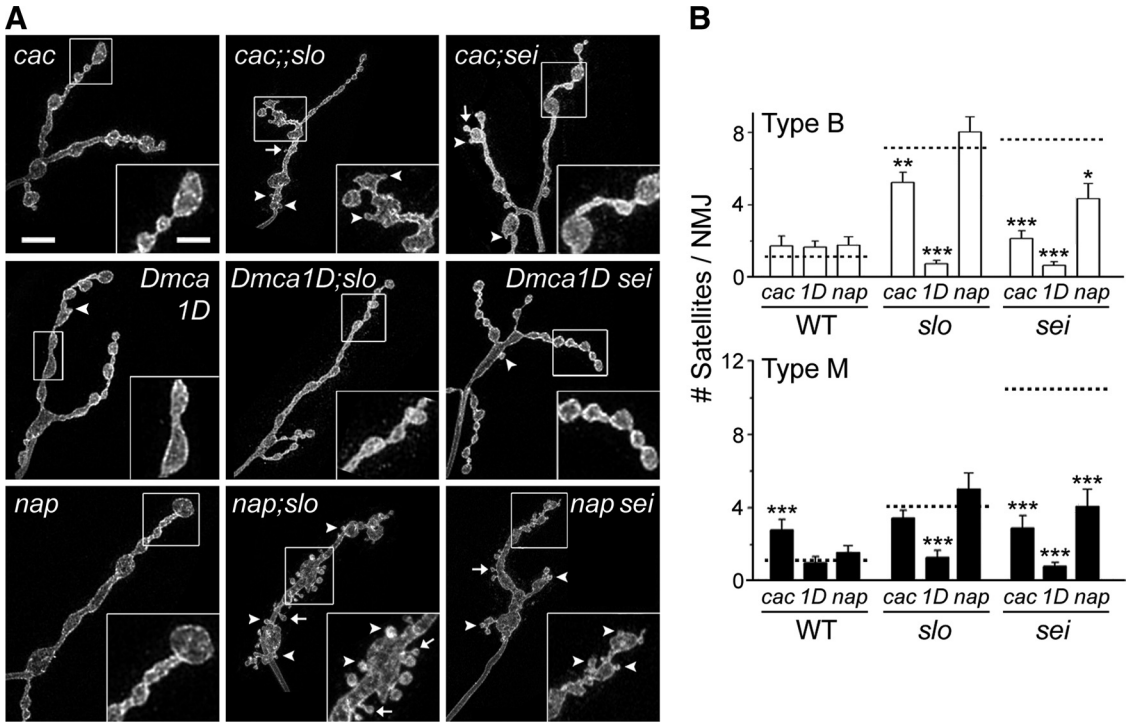

Figure 5. Ca^{2+}- and activity-dependent regulation of satellite formation in *slo* and *sei* mutants. ***A***, Typical synaptic bouton morphology of type Ib NMJs in muscle 4 for *cac*, *Dmca1D*, and *nap* single mutants and their double-mutant combinations with *slo* and *sei*. Scale bars: 10 μm; insets, 5 μm. Arrowheads and arrows show type B and M satellites, respectively. ***B***, Pooled data for type B (open) and M (closed) satellites are shown for *cac*, *Dmca1D* (*1D*), *nap*, and their double-mutant combinations with *slo* and *sei*. The corresponding control values from WT, *slo*, and *sei* larvae are indicated for each group (dashed lines, compare Fig. 1*C*). Note uniformly drastic suppression of satellites by *Dmca1D* in *Dmca1D;slo* and *Dmca1D sei* and selective suppression of satellite formation by *cac* and *nap* in the *sei*, but not *slo*, background, mirroring the contrasting effects of *dlg* and *fasII* (compare Fig. 4*C*). Numbers of NMJs (larvae) examined are as follows: *cac*, 19 (5); *Dmca1D*, 21 (5); *nap*, 20 (5); *cac;;slo,* 38 (10); *Dmca1D;slo*, 17 (4); *nap;slo*, 26 (6); *cac;sei*, 21 (5); *Dmca1D sei*, 32 (8); *nap sei*, 20 (5). $*p < 0.05$; $**p < 0.01$; $***p < 0.001$ (*t* test for WT, *slo*, or *sei* vs double mutants within each group). Error bars indicate mean ± SEM.

the similar outcomes for *slo*-induced satellite formation caused by two different treatments that facilitate synaptic growth.

Differential contributions of pre- and post-synaptic Ca^{2+} channels to satellite formation in *slo* and *sei* mutants

Dlg and its vertebrate homologs, including PSD-95, play important roles in scaffolding various post-synaptic proteins, such as FasII, glutamate receptor, and Sh K^+ channels (Lahey et al., 1994; Kim and Sheng, 2004), whereas pre-synaptic regulation of FasII is particularly important for growth plasticity at *Drosophila* larval NMJs (Schuster et al., 1996). Significantly, activity-dependent accumulation of intracellular Ca^{2+} has been implicated in modulation of both PSD-95 and FasII (Schuster et al., 1996; Kim and Sheng, 2004). The differential *dlg*- and *fasII*-dependent modulation (Fig. 4) thus may reflect distinct Ca^{2+} signaling processes, including Ca^{2+} channels, in regulation of *slo* and *sei* satellites.

Two genes, *Dmca1D* and *cacophony*, have been identified to encode voltage-activated Ca^{2+} channels in *Drosophila*. The Dmca1D channels, sharing homology to vertebrate L-type Ca^{2+} channels, are thought to be the predominant Ca^{2+} channels in post-synaptic muscles at NMJs (Zheng et al., 1995; Ren et al., 1998). In contrast, the Cac channels serve similar functions as vertebrate N-type channels, playing a major role in pre-synaptic neurotransmitter release (Smith et al., 1996; Kawasaki et al., 2000, 2002, 2004). Our double-mutant analysis indicated that separate pre- and post-synaptic actions of Cac and Dmca1D channels, respectively, exert differential influences on *slo* and *sei* satellites (Fig. 5). Since null mutations of these two Ca^{2+} channels are lethal, we used viable hypomorphic alleles to construct double mutants with *slo* and *sei* (see Materials and Methods). Nevertheless, the results showed clear suppressive effects on satellite formation in double-mutant combinations.

Significantly, the *Dmca1D* mutation suppressed both type B and M satellites in *Dmca1D;slo* and *Dmca1D sei* double mutants nearly to the WT level. This parallels with *dlg*-induced suppression of *slo* and *sei* satellites (compare Figs. 4*B* and 5*B*), suggesting a strong post-synaptic influence on the initial budding step (Fig. 1*E*, step a). Such suppression in satellite formation led to the morphology of *Dmca1D;slo* resembling that of *Dmca1D* single mutants (supplemental Table S1, available at www.jneurosci.org as supplemental material).

In contrast to *Dmca1D*, *cac*-induced suppression of satellite frequency was more drastic in *sei* than *slo* mutants, mirroring the *fasII* action (compare Figs. 4 and 5). Although *cac* mutations by themselves [cac^s (Fig. 5); cac^{NT27}/cac^s (data not shown)] caused no significant changes in the morphological parameters examined, except for an increase in type M satellites, *cac;sei* (but not *cac;;slo*) double mutants displayed drastic decreases in both type B and M satellites (Fig. 5*B*), along with even more pronounced reduction in the number of mature boutons and terminal branches (supplemental Table S1, supplemental Fig. S4A, available at www.jneurosci.org as supplemental material). These results thus suggest a tight functional relation of Sei, rather than Slo, K^+ channels with Cac pre-synaptic Ca^{2+} channels in regulation of Ca^{2+} influx for initial satellite formation as well as maturation (Fig. 1*E*, steps a–c).

Such tight association between Sei K^+ channels and pre-synaptic regulators of membrane excitability was further supported by the double-mutant phenotypes when the nap^{ts} ($maleless^{nap}$) mutation was combined with either *sei* or *slo*. The

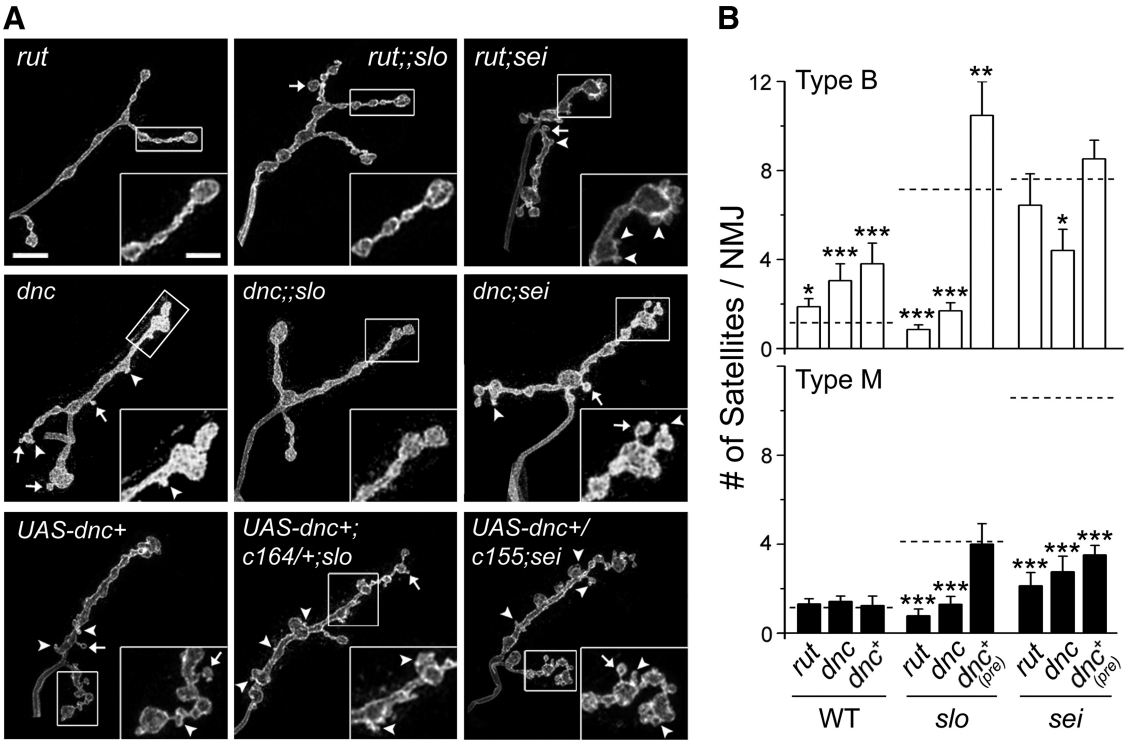

Figure 6. cAMP-dependent modulation of satellite formation in *slo* and *sei* mutants. ***A***, ***B***, Representative images of type Ib muscle 4 NMJs (***A***) and types B and M satellite frequencies (***B***) demonstrate the effects of the *rut* and *dnc* mutations and pre-synaptic expression of *dnc*-PDE (*UAS-dnc*$^+$) on *slo* and *sei* synaptic overgrowth. Note essentially complete suppression of satellites by Rut AC and Dnc PDE mutations in *rut;;slo* and *dnc;;slo*, respectively, but not by pre-synaptic expression of *dnc*$^+$ in the motor neurons [*dnc*$^+$ (pre) or *UAS-dnc*$^+$*;c164/+;slo*]. In contrast, *sei*-induced type M satellites are suppressed by both the *rut* and *dnc* mutations and pre-synaptically expressed PDE [*dnc*$^+$ (pre) or *UAS-dnc*$^+$*/c155;sei*]. (See Results for abundant type B satellites still remaining in *rut;sei*, *UAS-dnc*$^+$*/c155;sei*, and, to a lesser extent, *dnc;sei*.) The corresponding control values from WT, *slo*, and *sei* are indicated in ***B*** (dashed lines; compare Fig. 1*C*). Scale bars: 10 μm; insets, 5 μm. Arrowheads and arrows show type B and M satellites, respectively. The numbers of NMJs (larvae) examined are as follows: 34 (8) for *rut*; 21 (5) for *dnc*; 16 (4) for *UAS-dnc*$^+$; 14 (4) for *rut;;slo*; 20 (5) for *dnc;;slo*; 17 (4) for *UAS-dnc*$^+$*;c164/+;slo*; 16 (4) for *rut;sei*; 17 (4) for *dnc;sei*; 23 (6) for *UAS-dnc*$^+$*/c155;sei*. *$p < 0.05$; **$p < 0.01$; ***$p < 0.001$ (*t* test for WT, *slo*, or *sei* vs double mutants within each group). Error bars indicate mean ± SEM.

nap mutation down-regulates the *paralytic* (*para*) gene encoding voltage-activated Na^+ channels in *Drosophila*, weakening neuronal excitability and causing paralysis at high temperature (Wu et al., 1978; Kernan et al., 1991). Our results demonstrated suppression in satellite growth, in particular the type M, in *nap sei* double mutants (Fig. 5*B*). In contrast, the number of both types of satellites remained unchanged in *nap;slo* double mutants compared to *slo* single mutants (Fig. 5*B*). Since *Drosophila* muscle is devoid of Na^+ channels (Singh and Wu, 1999), reduced excitability by *nap* presumably affects only pre-synaptic growth regulation associated with Sei- but not Slo-associated post-synaptic mechanisms.

Role of cAMP in pre- and post-synaptic regulation of satellite formation

The preferential effects of *nap*, *cac*, and *Dmca1D* mutations in suppressing *sei* and *slo* satellites prompted us to examine the role of *rutabaga* adenylyl cyclase (AC) that produces cAMP in a Ca^{2+}/CaM-dependent manner (Livingstone et al., 1984; Levin et al., 1992). As reported previously, *rut* suppresses synaptic overgrowth induced by *eag Sh* hyperexcitability and HT treatments (Zhong et al., 1992; Zhong and Wu, 2004), but itself does not induce significant changes in the synaptic growth parameters, including the rare occurrence of satellites (Fig. 6; supplemental Table S1, available at www.jneurosci.org as supplemental material). Then, we examined the effects of *rut* mutations on *slo* and *sei* satellites using double-mutant combinations.

Despite their abundance in *slo* single mutants, both type B and M satellites were suppressed in *rut;;slo* double mutants to the WT level, along with a slight reduction in mature bouton number (Fig. 6; supplemental Table S1, available at www.jneurosci.org as supplemental material), paralleling the effects of *dlg* and *Dmca1D* mutations on satellite formation. In contrast to *rut;;slo* showing equal suppression, *rut;sei* double mutants displayed selective suppression of type M, but not type B, satellites (Fig. 6*B*), along with drastically reduced mature bouton (supplemental Table S1, available at www.jneurosci.org as supplemental material) and branch formation (supplemental Fig. S4B, available at www.jneurosci.org as supplemental material).

In parallel, we also examined the effects of mutations in *dunce* (*dnc*), a gene encoding a cAMP-specific phosphodiesterase (PDE) (Byers et al., 1981). Loss of PDE actions in *dnc* mutants results in accumulation of cAMP, in contrast to its depletion in *rut*. Despite such counteractive influences of *rut* and *dnc* mutations on cAMP metabolism, we found similar trends of changes in satellite frequency and overall bouton formation caused by *dnc* mutations. Significantly, *dnc;;slo* double mutants displayed drastic suppression of both types of satellites and mature boutons, in contrast to a relatively selective reduction in type M satellites and mature boutons in *dnc;sei* double mutants (Fig. 6; supplemental Table S1, available at www.jneurosci.org as supplemental material). These results thus suggest that fine-tuning of an optimal level, rather than a simple reduction or elevation, of cAMP is an important aspect of regulating satellite formation as well as overall synaptic growth. This is an interesting parallel to the previous reports that defects in cAMP synthesis or degradation caused by *rut* and *dnc*, respectively, can lead to similar abnormalities at

multiple levels, despite their opposite effects on cAMP concentration. These mutant phenotypes include poor learning ability of adult flies (Tully and Quinn, 1985), defects in growth cone morphology and motility (Kim and Wu, 1996) and disrupted spike-firing patterns (Zhao and Wu, 1997) in cultured embryonic neuroblasts, and impaired synaptic function at larval NMJs (Renger et al., 2000). Our study thus further supports the idea of "optimal cAMP levels" required for proper neuronal function and structure.

We further investigated differential effects of *rut* and *dnc* mutations on *slo* and *sei* satellites with targeted alterations of cAMP metabolism in the pre- and post-synaptic compartments using the GAL4-UAS expression system (Brand and Perrimon, 1993). Among the possible GAL4 and UAS lines to be introduced into the *slo* and *sei* mutant backgrounds, two combinations were selected for the ease of genetic schemes that allow targeted pre-synaptic expression of a wild-type *dnc* transgene (*UAS-dnc*$^+$). Since *dnc* PDE hydrolyzes cAMP, forced expression of PDE could lead to decreased cAMP levels, resembling *rut*-induced reduction in cAMP levels.

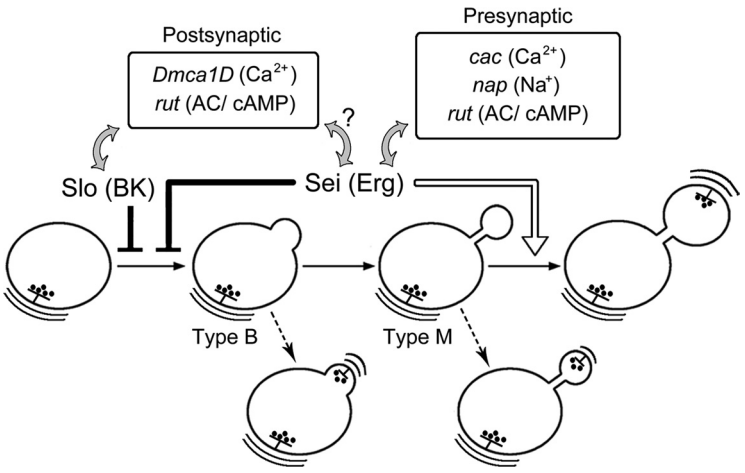

Figure 7. Model of a sequential growth process: Slo and Sei K^+ channels in regulation of synaptic growth by pre- and post-synaptic Ca^{2+} and cAMP. Our study suggests a sequential mode of synaptic growth process in which each step is differentially modulated by Slo (BK) and Sei (Erg) K^+ channels. Double-mutant analysis reveals separate sets of interactive partners of Sei and Slo channels. Through regulation of membrane excitability, Slo channels preferentially influence the functioning of the post-synaptic players, including *Dmca1D* Ca^{2+} channels, *dlg* (PSD), and *rut* AC/cAMP signaling (gray arrows). Although similar interaction may exist for Sei channels (arrow with a question mark), our results suggest a tight interaction between Sei channels and *cac* Ca^{2+} and *nap* Na^+ channels, FasII, and again *rut* AC/cAMP signaling situated in the pre-synaptic compartment (gray arrows) (see Results for Dlg, FasII, and other details). Induction of type B satellite formation involves both pre- and post-synaptic contributions and is normally restrained by both Slo and Sei channels (closed bar). Sei channels further promote a subsequent step of type B satellite maturation, from type M into primary synaptic boutons and branches (open arrow). Dysfunction of Sei and Slo channels leads to abundance of both types of satellites, representing the transient growth intermediates that are arrested or stabilized through ultrastructural differentiation (dashed arrows).

Interestingly, pre-synaptic expression of PDE (*UAS-dnc*$^+$ driven by pan-neuronal *C155-GAL4*) in the *sei* background closely mimicked the *rut* effects on *sei* satellite formation, i.e., drastically reduced type M, but not type B, satellites (Fig. 6*B*) along with a milder decrease in primary bouton (supplemental Table S1, available at www.jneurosci.org as supplemental material) and branch numbers (supplemental Fig. S4B, available at www.jneurosci.org as supplemental material). These results thus support a major effect of *sei* mutations that is associated with pre-synaptic cAMP regulation.

In contrast to *sei*, we found that in the *slo* background, pre-synaptic expression of PDE (*UAS-dnc*$^+$ driven by motoneuron-specific *C164-GAL4*) failed to phenocopy *rut;;slo* (Fig. 6*B*), consistent with confined cAMP-dependent regulatory mechanisms to the post-synaptic compartment in *slo* satellite formation. Indeed, post-synaptic *dnc*$^+$ expressed in *slo* was effective in suppression of both type B and M satellites (supplemental Fig. S5, available at www.jneurosci.org as supplemental material), comparable to those in *rut;;slo* double mutants (compare Fig. 6*B* and supplemental Fig. S5, available at www.jneurosci.org as supplemental material). However, the number of mature boutons remained higher in *slo* mutants expressing post-synaptic *dnc*$^+$ (supplemental Fig. S5; for *slo* and *rut;;slo*, see supplemental Table S1, available at www.jneurosci.org as supplemental material), indicating that the phenotypes of *rut;;slo* can be partially reproduced by overexpression of post-synaptic, but not pre-synaptic, *dnc*$^+$ in *slo* mutants.

It should be noted that differential suppression of *slo* and *sei* satellites by pre-synaptic PDE expression resembles the effects of *fasII* and *cac* mutations (compare Figs. 4, 5, 6). However, *rut*- and pre-synaptic *dnc*$^+$-induced suppression of *sei* satellites was restricted to type M satellites (Fig. 6*B*), whereas both *fasII* and *cac* mutations caused significant suppression of type M and, to a lesser extent, type B satellites in double-mutant combinations with *sei* (Figs. 4*C*, 5*B*). Therefore, the promotion of earlier growth steps in *sei* mutants (Fig. 2) may involve additional Ca^{2+}-activated signaling pathways, such as CaMKII and PKG, that are known to affect synaptic growth at larval NMJs (Wang et al., 1994; Renger et al., 1999).

Discussion

Sequential growth process revealed by preferential effects of BK and Erg K^+-channel mutations and the associated pre- and post-synaptic regulatory mechanisms

Distinct satellite patterns induced by *slo* and *sei* mutations support the notion that the two K^+ channels act on separate growth steps in concert with localized molecular partners. Our double-mutant analysis leads to a minimal model involving functional interactions of Slo and Sei K^+ channels with distinct assemblies of pre- and post-synaptic regulators in the sequential steps of synaptic growth and differentiation (Fig. 7). Expression of *slo* mutant phenotypes depends on scaffold protein, Dlg, and post-synaptic Dmca1D Ca^{2+} channels, both of which appear to be important for initial budding of satellites (Figs. 4, 5, 7). Double-mutant analysis reveals a tight association between Sei, but not Slo, K^+ channels and adhesion molecule, FasII, and pre-synaptic Cac Ca^{2+} and Para Na^+ channels in initial satellite formation as well as the ensuing process (Figs. 4, 5, 7). In the same vein, manipulations of pre-synaptic cAMP affect only *sei*-induced satellite formation, whereas *slo* satellites are more susceptible to modulations in post-synaptic cAMP signaling (Figs. 6, 7; supplemental Fig. S5, available at www.jneurosci.org as supplemental material).

Whereas these pre- and post-synaptic molecules can contribute to the initial growth of satellites in *slo* and *sei* mutants, they may also be important for further differentiation and stabilization of such intermediate structures. The stabilized satellites could accumulate over time and would facilitate their capture in fixed preparations. Our immunohistochemical and electron-microscopic analyses indicate that the majority of *slo* and *sei* sat-

ellites are well differentiated in molecular composition and ultrastructure (Figs. 3, 4; supplemental Fig. S1, available at www.jneurosci.org as supplemental material). As live imaging studies have demonstrated, differentiation of early "ghost boutons" occurs at a slow rate, taking hours to days (Ataman et al., 2008). Consistently, our preliminary live imaging indicates type B and M satellites abundant in mutants as stable structures with no active morphological changes over the observation period up to 1 h, during which new satellites were sighted budding from primary boutons after high K^+ stimulation (data not shown). Thus, the synaptic differentiation process involving Slo or Sei K^+ channels and their interacting partners may occur at a slower time scale (Fig. 7, dashed arrows).

Our results demonstrate a more profound influence of post-synaptic molecules on initial induction of satellite formation and major pre-synaptic contribution in subsequent steps (Fig. 7). This picture is in line with potential retrograde signaling during the sequential growth process. Recent studies at *Drosophila* larval NMJs have revealed significant contributions of retrograde factors, such as bone morphogenetic protein, to synaptic development and function (Keshishian and Kim, 2004). It will be important to examine whether and how these factors take part in particular steps of the proposed sequential growth process.

Separate interacting partners of BK and Erg K^+ channels in regulation of synaptic growth

There has been emerging evidence for colocalization of post-synaptic BK channels with L-type Ca^{2+} channels (Hui et al., 1991) and with PSD-95 scaffold protein (Sailer et al., 2006) at vertebrate synapses. Our genetic analysis thus demonstrates the functional significance of the homologous post-synaptic macromolecular association (Slo BK, Dmca1D/L-type Ca^{2+} channels, and Dlg/PSD-95) in synaptic growth at the *Drosophila* NMJ. Whether interactions among these players are also important for regulation of synaptic transmission awaits further investigations.

It has been shown that sei^{ts1} mutants display increased spontaneous activities in the giant-fiber neuron (Elkins and Ganetzky, 1990) and enhanced synaptic growth at larval NMJs (Guan et al., 2005) when exposed to high temperature. However, we observed synaptic overgrowth even at room temperature in sei^{ts2} (Fig. 1) and, to a lesser extent, sei^{ts2}/sei^{ts1} (data not shown). DNA sequencing predicts truncated versus full-length polypeptides in the sei^{ts1} and sei^{ts2} alleles, respectively (Titus et al., 1997; Wang et al., 1997), which could explain the observed allele-dependent differences. Notably, altered pre-synaptic Ca^{2+} and cAMP regulation drastically suppressed *sei* phenotypes, but was ineffective on *slo*-induced overgrowth (Figs. 5, 6), suggesting significant interactions between Erg K^+ channels and these pre-synaptic components, although pre-synaptic interaction of the Sei K^+ channel with the Ca^{2+}/cAMP pathway has not been well established in *Drosophila*. DNA sequence analysis suggests a putative cyclic nucleotide-binding domain in Sei K^+ channels, similar to Eag that belongs to the same K^+-channel family (Wang et al., 1997). Whether cAMP-dependent modification of *sei* phenotypes (Fig. 6) is related to the action of this putative domain should be further investigated in future studies.

Multimeric assembly and transgenic manipulations of Slo and Sei K^+ channels

Multimeric assembly of K^+ channels, including Sei Erg and Slo BK, has been implicated in regulating the channel properties (Hille, 2001). Indeed, sei^{ts2}/+ and *slo*/+ larvae, presumably containing a mixture of mutated and WT subunits in their Erg and BK channels, display dominant mutational effects on satellite formation and associated synaptic growth (supplemental Table S2, available at www.jneurosci.org as supplemental material). Importantly, pre-synaptic expression of a mutated *sei* transgene (*UAS-*sei^{ts2}) in WT led to a similar, but less extreme, phenotype (supplemental Table S2, available at www.jneurosci.org as supplemental material), confirming the pre-synaptic action of sei^{ts2} and its dominant effects in multimeric Sei channels.

It is interesting to ask whether simply reducing the amount of Sei and Slo channel proteins may produce phenotypes similar to heterozygous sei^{ts2}/+ and *slo*/+ animals. We employed the RNA interference (RNAi) technique to test this possibility, using multiple combinations of GAL4 drivers and UAS-*slo*/*sei*-RNAi constructs, with Dicer-2 to facilitate RNA interference in some combinations (Lee et al., 2004; Pham et al., 2004) (supplemental Table S3, available at www.jneurosci.org as supplemental material). However, none of these combinations caused characteristic behavioral and physiological abnormalities of *sei* and *slo* (Jackson et al., 1984; Elkins et al., 1986; Elkins and Ganetzky, 1990; Gho and Ganetzky, 1992; Warbington et al., 1996; Atkinson et al., 2000; Lee, 2008; Lee et al., 2008). We observed only marginal and inconsistent synaptic growth phenotypes among these combinations. For instance, the expression of *slo* and *sei* RNAi in motoneurons with the driver *C164-GAL4* led to a slightly elevated satellite frequency, but the pan-neuronal driver *C155-GAL4* produced even less overgrowth. Bouton formation was enhanced in these GAL4-UAS-RNAi combinations but not significantly above the elevated levels intrinsic to individual GAL4 and RNAi lines (supplemental Table S3, available at www.jneurosci.org as supplemental material).

The results suggest that dysfunctions induced by RNAi knockdown may not reproduce all aspects of mutant phenotypes. A match in protein levels or altered protein properties may be required to produce the phenotype of interest. At this time, the efficiency of these RNAi lines has not been documented. Since we were unable to measure the levels of Slo and Sei proteins because of a lack of appropriate antibodies, it is not possible to determine the levels of each RNAi knockdown. The *slo* and *sei* mutations induced by a chemical mutagen, ethyl methanesulfonate, may affect the properties and/or the amount of the gene product. For example, sei^{ts2} mutants carry a point mutation near the pore domain of the channels (Titus et al., 1997; Wang et al., 1997), and thus may act as neomorphs that confer dominant effects in the heterozygote, a property difficult to be mimicked by RNAi knockdown.

cAMP-dependent regulation of synaptic overgrowth induced by BK and Erg K^+-channel dysfunction

Our results point out the critical role of cAMP signaling in the expression of both *slo* and *sei* mutant phenotypes (Fig. 7) and further highlight the profound functional consequences of altered excitability in neuronal plasticity. Activation of *rut* AC by activity-dependent accumulation of intracellular Ca^{2+} is pivotal in several forms of synaptic plasticity. For instance, in the *Aplysia* siphon-gill withdrawal reflex model, sensitizing stimuli increase cAMP levels and subsequently enhance transmission efficacy at sensorimotor synapses (Bernier et al., 1982), and repeated conditioning induces sensory varicosity growth (Bailey and Chen, 1983). Similarly, cAMP-dependent activation of protein kinase A in hippocampal slices is required for late-phase LTP that involves formation of new dendritic spines (Nguyen and Kandel, 1996).

At *Drosophila* larval NMJs, altered cAMP metabolism in *rut* and *dnc* mutants impairs synaptic transmission stability (Renger et al., 2000) and post-tetanic potentiation (Zhong and Wu,

1991). In addition, fewer docked vesicles (Renger et al., 2000) and retarded reserve pool mobilization (Kuromi and Kidokoro, 2000) have been documented in these mutants, indicating vesicle targeting and cycling defects. Thus, it will be interesting to examine the possibility that suppression of *slo* and *sei* satellites by *rut* is associated with alterations in membrane recycling. Such studies can be facilitated by relevant mutations, such as *shibire* defective in Dynamin, which is responsible for vesicle pinch-off (Koenig and Ikeda, 1983; Kim and Wu, 1987; Stimson and Ramaswami, 1999), or *drp1* (Dynamin-related protein 1) defective in reserve pool mobilization (Verstreken et al., 2005).

In summary, our observations reveal distinct patterns of satellite formation induced by *sei* and *slo* mutations affecting two separate categories of K^+ channels, which are apparently regulated by pre- and post-synaptic Ca^{2+}/cAMP signaling, respectively. Together with previous studies, convergence on the Ca^{2+}/CaM-activated cAMP synthesis by *rut* AC in the regulation of synaptic growth induced by a variety of K^+ channel mutations (Budnik et al., 1990; Zhong et al., 1992; Zhong and Wu, 2004) further establishes a central role of *rut* AC in activity-dependent plasticity of synaptic function and growth.

References

Ataman B, Ashley J, Gorczyca M, Ramachandran P, Fouquet W, Sigrist SJ, Budnik V (2008) Rapid activity-dependent modifications in synaptic structure and function require bidirectional Wnt signaling. Neuron 57:705–718.

Atkinson NS, Robertson GA, Ganetzky B (1991) A component of calcium-activated potassium channels encoded by the *Drosophila* slo locus. Science 253:551–555.

Atkinson NS, Brenner R, Chang W, Wilbur J, Larimer JL, Yu J (2000) Molecular separation of two behavioral phenotypes by a mutation affecting the promoters of a Ca-activated K channel. J Neurosci 20:2988–2993.

Atwood HL, Govind CK, Wu CF (1993) Differential ultrastructure of synaptic terminals on ventral longitudinal abdominal muscles in *Drosophila* larvae. J Neurobiol 24:1008–1024.

Bailey CH, Chen M (1983) Morphological basis of long-term habituation and sensitization in *Aplysia*. Science 220:91–93.

Bastiani MJ, Harrelson AL, Snow PM, Goodman CS (1987) Expression of fasciclin I and II glycoproteins on subsets of axon pathways during neuronal development in the grasshopper. Cell 48:745–755.

Bernier L, Castellucci VF, Kandel ER, Schwartz JH (1982) Facilitatory transmitter causes a selective and prolonged increase in adenosine 3′:5′-monophosphate in sensory neurons mediating the gill and siphon withdrawal reflex in *Aplysia*. J Neurosci 2:1682–1691.

Brand AH, Perrimon N (1993) Targeted gene expression as a means of altering cell fates and generating dominant phenotypes. Development 118:401–415.

Budnik V, Zhong Y, Wu CF (1990) Morphological plasticity of motor axons in *Drosophila* mutants with altered excitability. J Neurosci 10:3754–3768.

Byers D, Davis RL, Kiger JA Jr (1981) Defect in cyclic AMP phosphodiesterase due to the dunce mutation of learning in *Drosophila* melanogaster. Nature 289:79–81.

Chiang RG, Govind CK (1986) Reorganization of synaptic ultrastructure at facilitated lobster neuromuscular terminals. J Neurocytol 15:63–74.

Coyle IP, Koh YH, Lee WC, Slind J, Fergestad T, Littleton JT, Ganetzky B (2004) Nervous wreck, an SH3 adaptor protein that interacts with Wsp, regulates synaptic growth in *Drosophila*. Neuron 41:521–534.

Dickman DK, Lu Z, Meinertzhagen IA, Schwarz TL (2006) Altered synaptic development and active zone spacing in endocytosis mutants. Curr Biol 16:591–598.

Elkins T, Ganetzky B (1990) Conduction in the giant nerve fiber pathway in temperature-sensitive paralytic mutants of *Drosophila*. J Neurogenet 6:207–219.

Elkins T, Ganetzky B, Wu CF (1986) A *Drosophila* mutation that eliminates a calcium-dependent potassium current. Proc Natl Acad Sci U S A 83:8415–8419.

Engert F, Bonhoeffer T (1999) Dendritic spine changes associated with hippocampal long-term synaptic plasticity. Nature 399:66–70.

Gho M, Ganetzky B (1992) Analysis of repolarization of presynaptic motor terminals in *Drosophila* larvae using potassium-channel-blocking drugs and mutations. J Exp Biol 170:93–111.

Gossett LA, Kelvin DJ, Sternberg EA, Olson EN (1989) A new myocyte-specific enhancer-binding factor that recognizes a conserved element associated with multiple muscle-specific genes. Mol Cell Biol 9:5022–5033.

Guan Z, Saraswati S, Adolfsen B, Littleton JT (2005) Genome-wide transcriptional changes associated with enhanced activity in the *Drosophila* nervous system. Neuron 48:91–107.

Haugland FN, Wu CF (1990) A voltage-clamp analysis of gene-dosage effects of the Shaker locus on larval muscle potassium currents in *Drosophila*. J Neurosci 10:1357–1371.

Hille B (2001) Ion channels of excitable membranes, Ed 3. Sunderland, MA: Sinauer Associates.

Hui A, Ellinor PT, Krizanova O, Wang JJ, Diebold RJ, Schwartz A (1991) Molecular cloning of multiple subtypes of a novel rat brain isoform of the alpha 1 subunit of the voltage-dependent calcium channel. Neuron 7:35–44.

Jackson FR, Wilson SD, Strichartz GR, Hall LM (1984) Two types of mutants affecting voltage-sensitive sodium channels in *Drosophila* melanogaster. Nature 308:189–191.

Jackson FR, Gitschier J, Strichartz GR, Hall LM (1985) Genetic modifications of voltage-sensitive sodium channels in *Drosophila*: gene dosage studies of the seizure locus. J Neurosci 5:1144–1151.

Jan LY, Jan YN (1976) Properties of the larval neuromuscular junction in *Drosophila* melanogaster. J Physiol 262:189–214.

Johansen J, Halpern ME, Johansen KM, Keshishian H (1989) Stereotypic morphology of glutamatergic synapses on identified muscle cells of *Drosophila* larvae. J Neurosci 9:710–725.

Kawasaki F, Felling R, Ordway RW (2000) A temperature-sensitive paralytic mutant defines a primary synaptic calcium channel in *Drosophila*. J Neurosci 20:4885–4889.

Kawasaki F, Collins SC, Ordway RW (2002) Synaptic calcium-channel function in *Drosophila*: analysis and transformation rescue of temperature-sensitive paralytic and lethal mutations of cacophony. J Neurosci 22:5856–5864.

Kawasaki F, Zou B, Xu X, Ordway RW (2004) Active zone localization of presynaptic calcium channels encoded by the cacophony locus of *Drosophila*. J Neurosci 24:282–285.

Kernan MJ, Kuroda MI, Kreber R, Baker BS, Ganetzky B (1991) napts, a mutation affecting sodium channel activity in *Drosophila*, is an allele of mle, a regulator of X chromosome transcription. Cell 66:949–959.

Keshishian H, Kim YS (2004) Orchestrating development and function: retrograde BMP signaling in the *Drosophila* nervous system. Trends Neurosci 27:143–147.

Kim E, Sheng M (2004) PDZ domain proteins of synapses. Nat Rev Neurosci 5:771–781.

Kim YT, Wu CF (1987) Reversible blockage of neurite development and growth cone formation in neuronal cultures of a temperature-sensitive mutant of *Drosophila*. J Neurosci 7:3245–3255.

Kim YT, Wu CF (1996) Reduced growth cone motility in cultured neurons from *Drosophila* memory mutants with a defective cAMP cascade. J Neurosci 16:5593–5602.

Koenig JH, Ikeda K (1983) Evidence for a presynaptic blockage of transmission in a temperature-sensitive mutant of *Drosophila*. J Neurobiol 14:411–419.

Koh TW, Verstreken P, Bellen HJ (2004) Dap160/intersectin acts as a stabilizing scaffold required for synaptic development and vesicle endocytosis. Neuron 43:193–205.

Kohsaka H, Takasu E, Nose A (2007) *In vivo* induction of postsynaptic molecular assembly by the cell adhesion molecule Fasciclin2. J Cell Biol 179:1289–1300.

Komatsu A, Singh S, Rathe P, Wu CF (1990) Mutational and gene dosage analysis of calcium-activated potassium channels in *Drosophila*: correlation of micro- and macroscopic currents. Neuron 4:313–321.

Kuromi H, Kidokoro Y (2000) Tetanic stimulation recruits vesicles from reserve pool via a cAMP-mediated process in *Drosophila* synapses. Neuron 27:133–143.

Lahey T, Gorczyca M, Jia XX, Budnik V (1994) The *Drosophila* tumor suppressor gene dlg is required for normal synaptic bouton structure. Neuron 13:823–835.

Lee J (2008) Effects of potassium and calcium channel mutations on synap-

tic function and growth at *Drosophila* larval neuromuscular junctions. PhD thesis, University of Iowa.

Lee J, Ueda A, Wu CF (2008) Pre- and post-synaptic mechanisms of synaptic strength homeostasis revealed by Slowpoke and Shaker K+ channel mutations in *Drosophila*. Neuroscience 154:1283–1296.

Lee YS, Nakahara K, Pham JW, Kim K, He Z, Sontheimer EJ, Carthew RW (2004) Distinct roles for *Drosophila* Dicer-1 and Dicer-2 in the siRNA/miRNA silencing pathways. Cell 117:69–81.

Levin LR, Han PL, Hwang PM, Feinstein PG, Davis RL, Reed RR (1992) The *Drosophila* learning and memory gene rutabaga encodes a Ca2+/Calmodulin-responsive adenylyl cyclase. Cell 68:479–489.

Lilly B, Galewsky S, Firulli AB, Schulz RA, Olson EN (1994) D-MEF2: a MADS box transcription factor expressed in differentiating mesoderm and muscle cell lineages during *Drosophila* embryogenesis. Proc Natl Acad Sci U S A 91:5662–5666.

Livingstone MS, Sziber PP, Quinn WG (1984) Loss of calcium/calmodulin responsiveness in adenylate cyclase of rutabaga, a *Drosophila* learning mutant. Cell 37:205–215.

Lnenicka GA, Atwood HL, Marin L (1986) Morphological transformation of synaptic terminals of a phasic motoneuron by long-term tonic stimulation. J Neurosci 6:2252–2258.

Marie B, Sweeney ST, Poskanzer KE, Roos J, Kelly RB, Davis GW (2004) Dap160/intersectin scaffolds the periactive zone to achieve high-fidelity endocytosis and normal synaptic growth. Neuron 43:207–219.

McFarlane S, Pollock NS (2000) A role for voltage-gated potassium channels in the outgrowth of retinal axons in the developing visual system. J Neurosci 20:1020–1029.

Nguyen PV, Kandel ER (1996) A macromolecular synthesis-dependent late phase of long-term potentiation requiring cAMP in the medial perforant pathway of rat hippocampal slices. J Neurosci 16:3189–3198.

Peckol EL, Zallen JA, Yarrow JC, Bargmann CI (1999) Sensory activity affects sensory axon development in *C. elegans*. Development 126:1891–1902.

Pham JW, Pellino JL, Lee YS, Carthew RW, Sontheimer EJ (2004) A Dicer-2-dependent 80s complex cleaves targeted mRNAs during RNAi in *Drosophila*. Cell 117:83–94.

Ren D, Xu H, Eberl DF, Chopra M, Hall LM (1998) A mutation affecting dihydropyridine-sensitive current levels and activation kinetics in *Drosophila* muscle and mammalian heart calcium channels. J Neurosci 18:2335–2341.

Renger JJ, Yao WD, Sokolowski MB, Wu CF (1999) Neuronal polymorphism among natural alleles of a cGMP-dependent kinase gene, foraging, in *Drosophila*. J Neurosci 19:RC28.

Renger JJ, Ueda A, Atwood HL, Govind CK, Wu CF (2000) Role of cAMP cascade in synaptic stability and plasticity: ultrastructural and physiological analyses of individual synaptic boutons in *Drosophila* memory mutants. J Neurosci 20:3980–3992.

Roos J, Kelly RB (1998) Dap160, a neural-specific Eps15 homology and multiple SH3 domain-containing protein that interacts with *Drosophila* dynamin. J Biol Chem 273:19108–19119.

Sacco T, Bruno A, Wanke E, Tempia F (2003) Functional roles of an ERG current isolated in cerebellar Purkinje neurons. J Neurophysiol 90:1817–1828.

Sailer CA, Kaufmann WA, Kogler M, Chen L, Sausbier U, Ottersen OP, Ruth P, Shipston MJ, Knaus HG (2006) Immunolocalization of BK channels in hippocampal pyramidal neurons. Eur J Neurosci 24:442–454.

Salkoff L, Butler A, Ferreira G, Santi C, Wei A (2006) High-conductance potassium channels of the SLO family. Nat Rev Neurosci 7:921–931.

Sanguinetti MC, Jiang C, Curran ME, Keating MT (1995) A mechanistic link between an inherited and an acquired cardiac arrhythmia: HERG encodes the IKr potassium channel. Cell 81:299–307.

Schuster CM, Davis GW, Fetter RD, Goodman CS (1996) Genetic dissection of structural and functional components of synaptic plasticity. I. Fasciclin II controls synaptic stabilization and growth. Neuron 17:641–654.

Sigrist SJ, Reiff DF, Thiel PR, Steinert JR, Schuster CM (2003) Experience-dependent strengthening of *Drosophila* neuromuscular junctions. J Neurosci 23:6546–6556.

Singh S, Wu CF (1999) Ionic currents in larval muscles of *Drosophila*. Int Rev Neurobiol 43:191–220.

Smith LA, Wang X, Peixoto AA, Neumann EK, Hall LM, Hall JC (1996) A *Drosophila* calcium channel alpha1 subunit gene maps to a genetic locus associated with behavioral and visual defects. J Neurosci 16:7868–7879.

Stimson DT, Ramaswami M (1999) Vesicle recycling at the *Drosophila* neuromuscular junction. Int Rev Neurobiol 43:163–189.

Titus SA, Warmke JW, Ganetzky B (1997) The *Drosophila* erg K+ channel polypeptide is encoded by the seizure locus. J Neurosci 17:875–881.

Tully T, Quinn WG (1985) Classical conditioning and retention in normal and mutant *Drosophila* melanogaster. J Comp Physiol A Neuroethol Sens Neural Behav Physiol 157:263–277.

Verstreken P, Ly CV, Venken KJ, Koh TW, Zhou Y, Bellen HJ (2005) Synaptic mitochondria are critical for mobilization of reserve pool vesicles at *Drosophila* neuromuscular junctions. Neuron 47:365–378.

Wagh DA, Rasse TM, Asan E, Hofbauer A, Schwenkert I, Durrbeck H, Buchner S, Dabauvalle MC, Schmidt M, Qin G, Wichmann C, Kittel R, Sigrist SJ, Buchner E (2006) Bruchpilot, a protein with homology to ELKS/CAST, is required for structural integrity and function of synaptic active zones in *Drosophila*. Neuron 49:833–844.

Wang J, Renger JJ, Griffith LC, Greenspan RJ, Wu CF (1994) Concomitant alterations of physiological and developmental plasticity in *Drosophila* CaM kinase II-inhibited synapses. Neuron 13:1373–1384.

Wang XJ, Reynolds ER, Deak P, Hall LM (1997) The seizure locus encodes the *Drosophila* homolog of the HERG potassium channel. J Neurosci 17:882–890.

Warbington L, Hillman T, Adams C, Stern M (1996) Reduced transmitter release conferred by mutations in the slowpoke-encoded Ca2(+)-activated K+ channel gene of *Drosophila*. Invert Neurosci 2:51–60.

Wu CF, Ganetzky B, Jan LY, Jan YN, Benzer S (1978) A *Drosophila* mutant with a temperature-sensitive block in nerve conduction. Proc Natl Acad Sci U S A 75:4047–4051.

Zhao ML, Wu CF (1997) Alterations in frequency coding and activity dependence of excitability in cultured neurons of *Drosophila* memory mutants. J Neurosci 17:2187–2199.

Zheng W, Feng G, Ren D, Eberl DF, Hannan F, Dubald M, Hall LM (1995) Cloning and characterization of a calcium channel alpha 1 subunit from *Drosophila* melanogaster with similarity to the rat brain type D isoform. J Neurosci 15:1132–1143.

Zhong Y, Wu CF (1991) Altered synaptic plasticity in *Drosophila* memory mutants with a defective cyclic AMP cascade. Science 251:198–201.

Zhong Y, Wu CF (2004) Neuronal activity and adenylyl cyclase in environment-dependent plasticity of axonal outgrowth in *Drosophila*. J Neurosci 24:1439–1445.

Zhong Y, Budnik V, Wu CF (1992) Synaptic plasticity in *Drosophila* memory and hyperexcitable mutants: role of cAMP cascade. J Neurosci 12:644–651.

Zito K, Parnas D, Fetter RD, Isacoff EY, Goodman CS (1999) Watching a synapse grow: noninvasive confocal imaging of synaptic growth in *Drosophila*. Neuron 22:719–729.